Summary of AFIN Measurements on Atka Bay Landfast Sea Ice in 2011

- Field Report -

Mario Hoppmann[1,2], Marcel Nicolaus[1], Jölund Asseng[1]

[1]Alfred Wegener Institute of Polar and Marine Research, Am Handelshafen 12, 27570 Bremerhaven, Germany

[2]Jacobs University Bremen, Campus Ring 1, 28759 Bremen, Germany

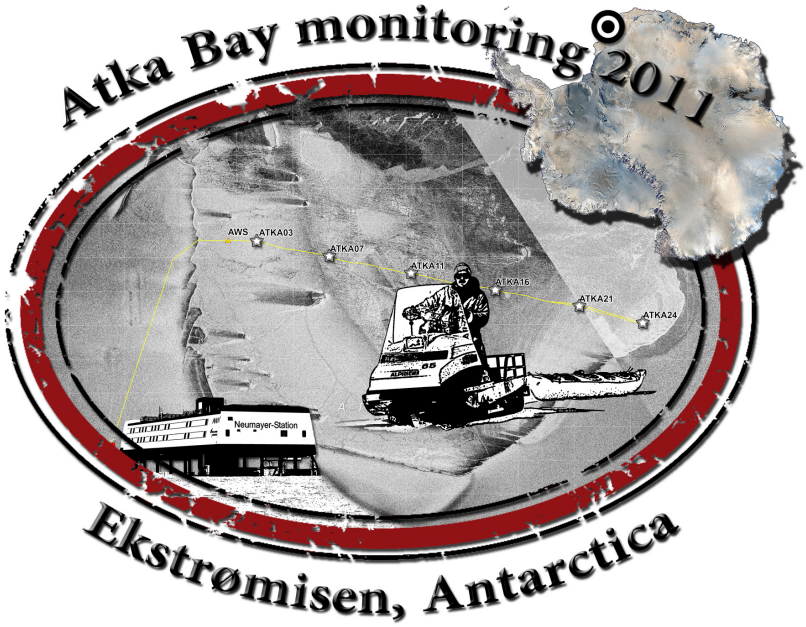

Alfred Wegener Institute for Polar and Marine Research

- 16 June 2012 -

Table of Contents

List of Figures

List of Tables

I
Introduction

Background

Antarctic sea-ice mass, -extent, and -properties are expected to experience significant changes in the next decades. Long-term and consistent time series of in-situ measurements are crucial to reveal insights into this system, and are needed to validate satellite derived sea-ice parameters and numerical simulations. Following the need for a coordinated approach on the monitoring of Antarctic landfast sea ice, the Antarctic Fast Ice Network (AFIN) was initiated as a legacy project during the 2007-2009 International Polar Year (Heil et al., 2011). As part of AFIN, a regular observation program was started in 2010 on the landfast sea ice of Atka Bay, in the northeastern Weddell Sea. The measurements are carried out by the German Antarctic station Neumayer III, situated on the Ekström Ice Shelf at 70°40'S, 008°16'W.

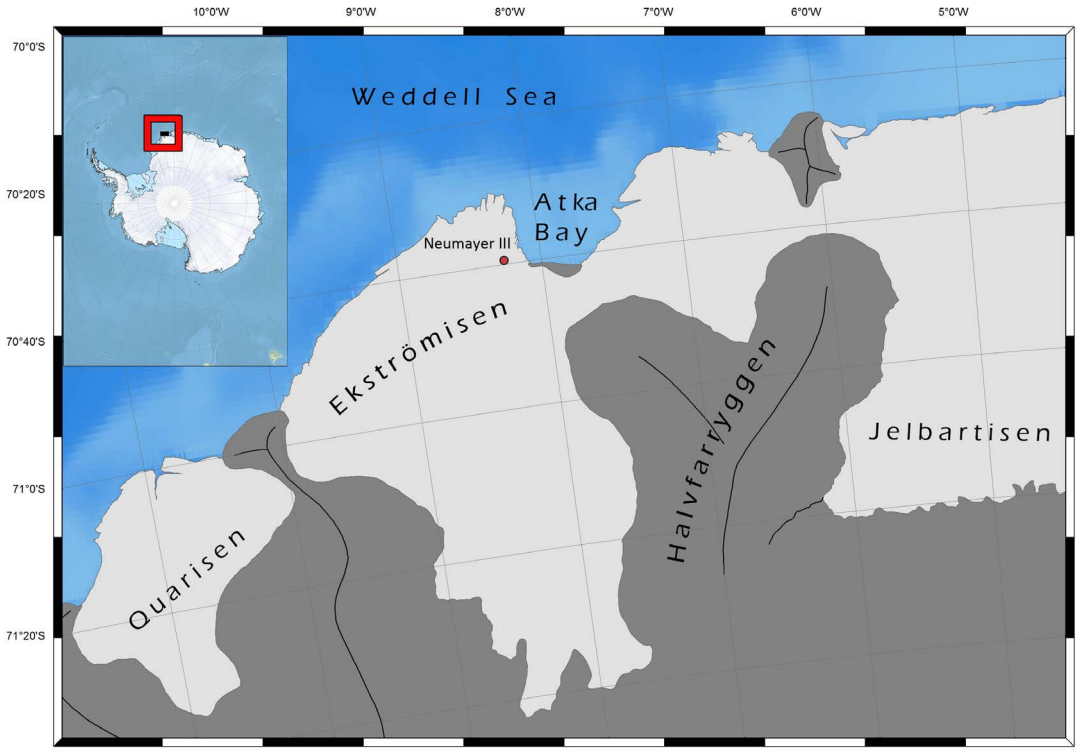

Figure 1: Study area

This field report describes our measurement activities between June 2011 and January 2012, and presents some preliminary results.

II

Methods and Results

In the previous year, the landfast sea ice of Atka Bay already broke off in early December. As a consequence, the stations in the northeast of Atka Bay could not be reached by snowmobile after 12 December 2010 (Hoppmann et al., 2011). In order to ensure a longer measurement period in 2011, we relocated the transect further south at the beginning of the measurement season (Figure 2).

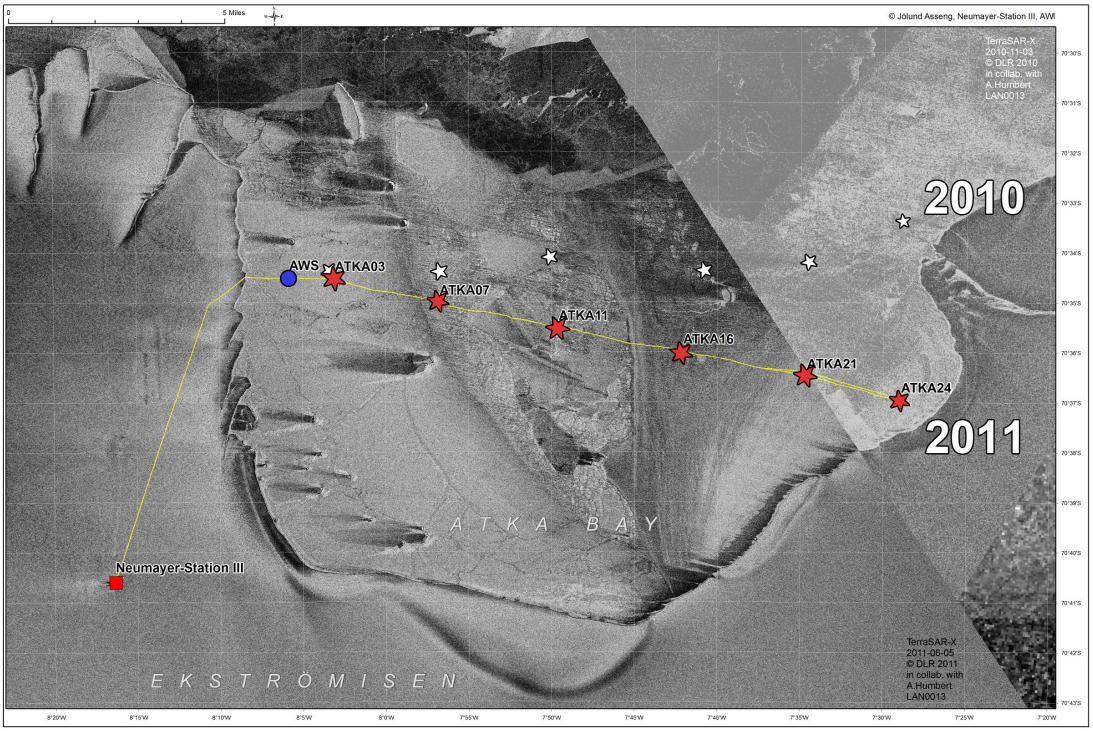

Figure 2: TerraSAR-X image of Atka Bay with stations of AFIN measurements in 2010 (white stars), 2011 (red stars) and the site of the automatic weather station and thermistor chain (blue dot). Station names (e.g. ATKA03) refer to the distance to the western ice-shelf edge.

2.1. Manual Thickness Measurements

We measured sea-ice thickness, snow depth and freeboard by repeated drill-hole measurements (5-cm diameter augers) between June 2011 and January 2012 (Table 1) at six stations distributed evenly over the transect across the Bay shown in Figure 2. The coordinates of these stations are given in Table 2. The equipment, including a generator and a heated box, was transported on snowmobiles and Nansen sleds (Figure 3)

Table 1: Dates of thickness measurements

Date	Drill-hole	EM31	Ice cores
06/06/2011	x		
01/07/2011	x		
04/08/2011	x		
19/08/2011	x		
14/09/2011	x		
09/10/2011	x		
30/10/2011	x		
18/11/2011	x	x	
29/11/2011		x	
11/12/2011	x	x	
29/12/2011	x	x	x
17/01/2012	x	x	x

Table 2: Coordinates of measuring stations in 2011

Station	Latitude	Longitude
AWS	70° 34.505' S	8° 05.753' W
ATKA03	70° 34.568' S	8° 03.055' W
ATKA07	70° 34.375' S	7° 56.727' W
ATKA11	70° 34.121' S	7° 50.187' W
ATKA16	70° 34.349' S	7° 40.873' W
ATKA21	70° 34.189' S	7° 34.632' W
ATKA24	70° 33.392' S	7° 28.947' W

During each measurement, 5 holes were drilled through the sea ice (Figure 4), one in the center and one in a distance of five meters in each direction, to cover the small-scale spatial variabilities. Snow depth and freeboard were measured with a ruler stick, and sea-ice thickness was determined with a custom-made pole (Figure 5). Temperatures of air (2 m), snow surface, snow, snow/sea-ice interface and water were measured by a hand held thermometer. In addition, photos of sea-ice conditions in each direction were taken, and the presence of ice platelets in the boreholes was documented.

Figure 3: Preparation of equipment

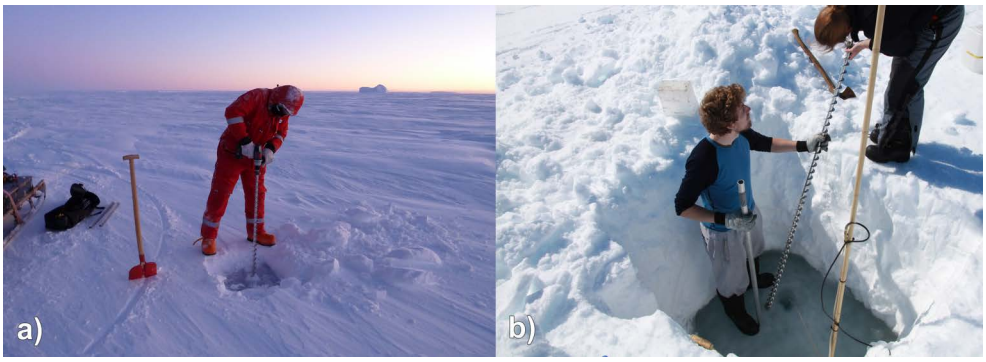

Figure 4: Manual drillings a) in thin snow; b) in thick snow

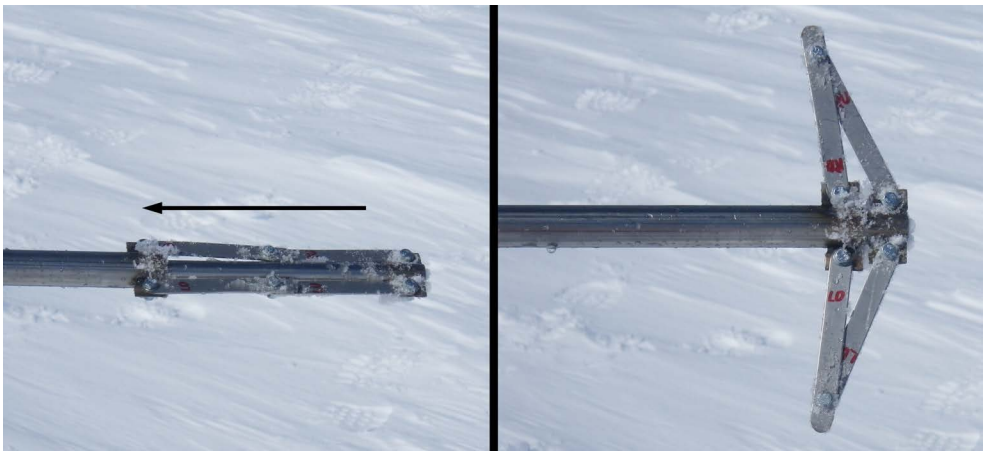

Figure 5: Custom-made pole to determine sea-ice thickness

Observations

The results of sea-ice thickness, freeboard and snow depths measurements are shown as time series in Figure 6 and as Hovmöller plots in Figure 7.

It can be inferred that from the beginning of June, **snow cover** is steadily increasing at all station except for ATKA24, where snow depth nearly stays constant. Most of the snow is accumulated between June and October, but it is quickly redistributed westwards due to persisting easterly winds (Figure 17). From November on, snow depths is declining again at all stations.

At the beginning of our field work at 06 June 2011, **sea-ice thickness** was already well over 80 cm at ATKA03, and over 50 cm at ATKA24. It increased quickly to an approximate thickness of 130-150 cm in September, when growth rates started to decline. The thickest sea ice was found regularly at ATKA07 throughout the entire season, with the highest small scale spatial variability. The maximum of 242 cm was found on 11 December 2011 at ATKA07.

Freeboard was highly variable during the season. At ATKA 03, the heavy snow cover of 80+ cm depressed the sea-ice surface under water level from July onwards, whereas at ATKA07 freeboard stayed positive all the season due to the very thick ice. At ATKA11, ATKA16 and ATKA21, freeboard was constantly negative since September, whereas it stayed positive at ATKA24 from August onwards due to the thin snow cover.

Table 3 shows the occurrence of ice platelets in boreholes since 19 August. In approximately every second borehole, platelets were observed. They were never found in boreholes at ATKA07, where the sea ice was thickest throughout. The lowest numbers were encountered in August, November and beginning of December. Platelets were found in nearly every hole drilled on 29 December 2011 and 17 January 2012(except at ATKA07).

Table 3: Occurrence of ice platelets in boreholes. The numbers indicate in how many of the five boreholes at each station ice platelets were found. s means small platelets, "-" indicates that no observation is available. On 11 September, further measurements had to be canceled due to bad weather. At ATKA24, the seawater had a distinct brown color, an indication of a diatom bloom (b).

	19.8	**11.9**	**14.9**	**9.10**	**30.10**	**18.11**	**11.12**	**29.12**	**17.1**
ATKA03	4	3	3	4	0	1	0	4	5
ATKA07	0	-	0	0	0	0	0	0	slush
ATKA11	3	-	0	4	5/s	2	4	5	5
ATKA16	0	-	5	1/s	5/s	0	2	4	5
ATKA21	2	-	4	3	5	0	1	3	5
ATKA24	0	-	5	2/s	4/b	b	0	5 /b	5/b

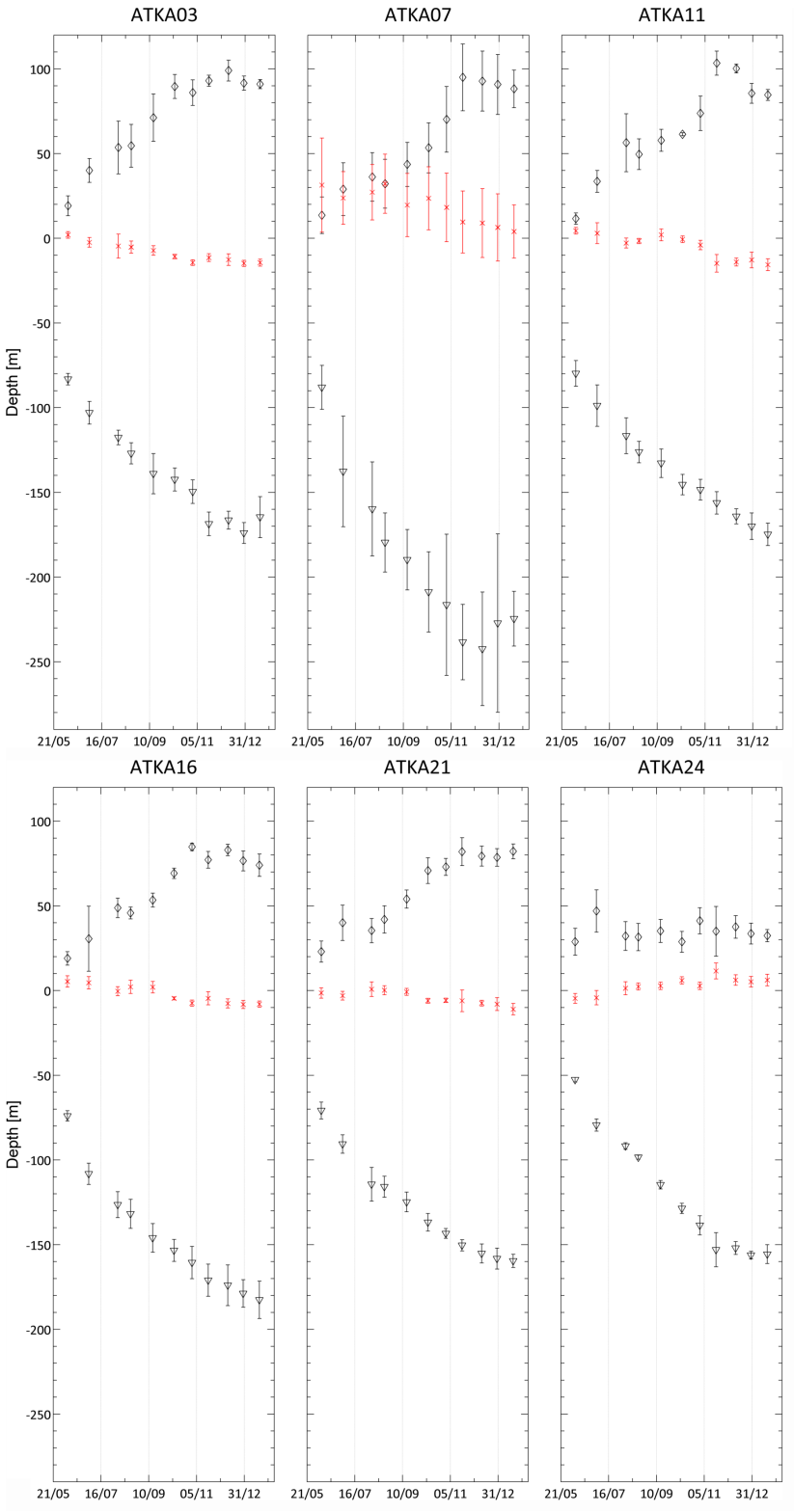

Figure 6: Results of manual drillings in 2011. The graph shows mean values of sea-ice thickness (black triangles), snow depth (black diamonds) and freeboard (red crosses). The error bars represent one standard deviation.

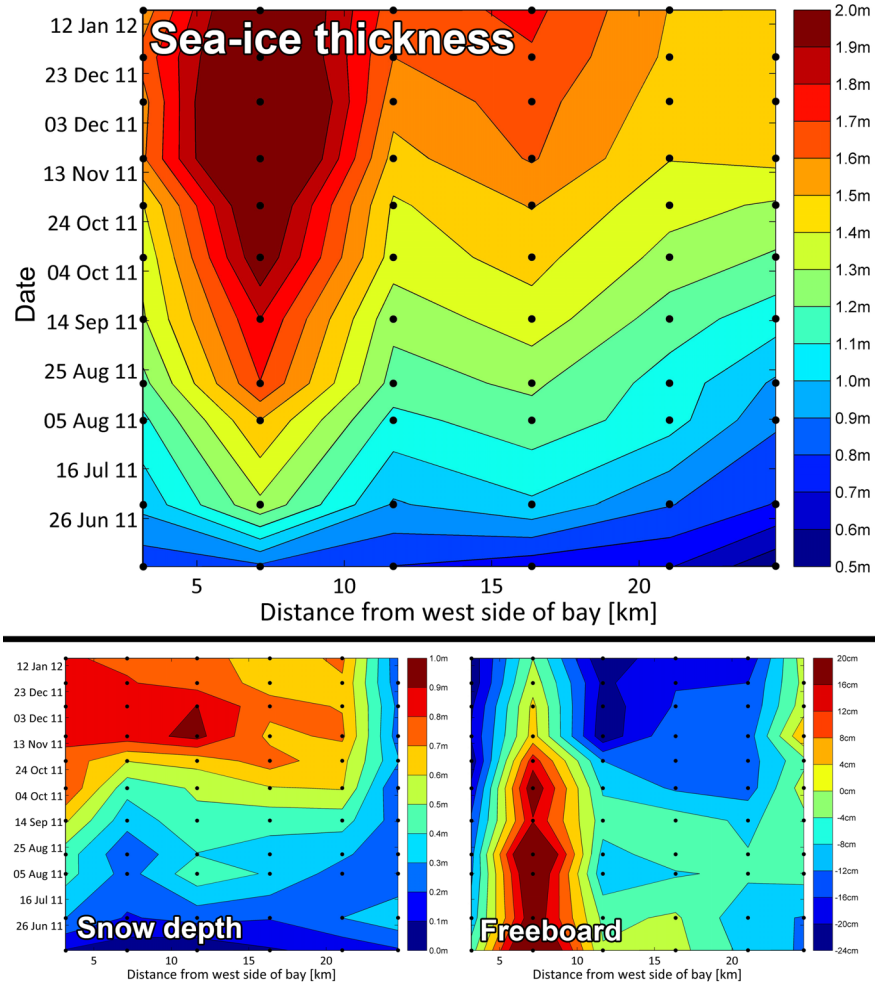

Figure 7: Contour plots of manual drillings in 2011

2.2. Electromagnetic Thickness Measurements (EM31)

Starting in November 2011, electromagnetic sea-ice thickness profiles along the transect shown in Figure 2 were obtained by an EM31 mounted in a kayak, and pulled behind a snowmobile (Figure 8).

Principle

The EM31 uses the emission and reception of Very Low Frequency (VLF) Electro Magnetic (EM) fields to determine the distribution of conductive layers. A time-harmonic EM-field (primary field) is generated by a transmitter coil, which induces currents in every conductive medium, leading to the formation of a secondary field. The sum of both primary and secondary field is subsequently detected at the receiver coil of the instrument.

In the so-called "1D Approximation", the electrical conductivities of sea ice and snow are neglected, and air can be seen as a perfect electrical insulator. As a result, only two effective media remain: the conductive sea water and the combined resistive layers of sea ice, snow and air.

In the case of the EM31, the apparent conductivity σ_a is used to calculate the distance to the sea ice/ocean interface h (Hendricks, 2009). At a given distance, the expected value of σ_a can be approximated by an exponential function of the kind

$$\sigma_a = A \cdot e^{B \cdot h} + C \tag{1}$$

Figure 8: EM31 pulled behind snowmobile

The EM31 was operated in Vertical CoPlanar (VCP) mode (Figure 9a), where the coil plane is oriented perpendicular to the surface.

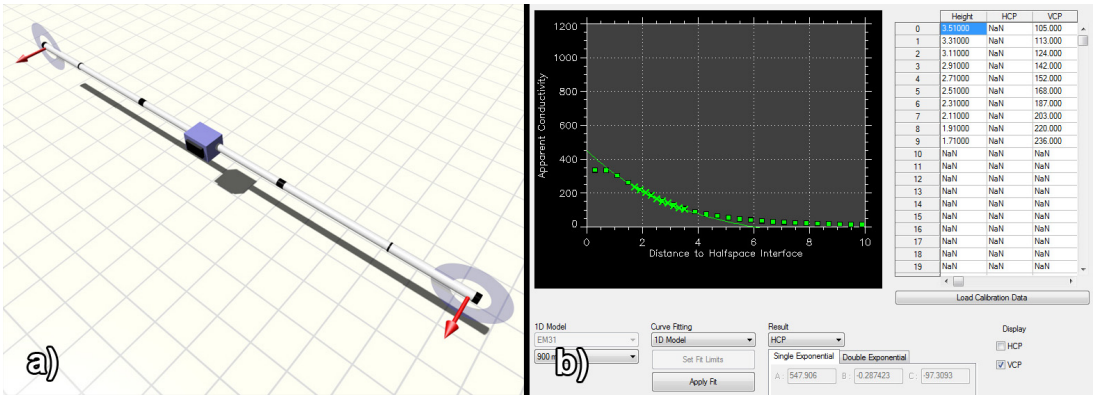

Figure 9: EM31: a) VCP mode (Hendricks, 2009); b) Calibration curve;

Our calibration yielded the exponential function (Figure 9b)

$$\sigma_a = 548.91 \cdot e^{-0.287 \cdot h} - 97.31, \tag{2}$$

where h = distance between coils and conductive medium, σ_a = apparent conductivity.

Total thickness is calculated by solving this equation for h, and by subtracting the distance between the coils and the snow surface.

As these data only reveal the total thickness of snow plus sea ice, additional ruler-stick measurements of snow depth were recorded in parallel. EM31 measurements along the profile defined in Figure 2 were performed on 18 November 2011, 12 December 2011, 29 December 2011 and 17 January 2012. On 29 November 2011, an additional grid covering a total of 114 km was recorded (see Table 1). During this measurement, communication problems with the GPS arose, leading to GPS data loss along two sections during the grid. Positioning data from a second GPS device were later integrated into the EM31 data by linear interpolation of position recording and synchronization of the time stamp.

Observations

The results of EM31 total thickness measurements are shown in Figures 10 and 11. The data show evidences of ridging in the middle part of the Bay, and confirm the lack of snow in the far eastern part. Furthermore, peaks in snow depths can not only be found in the West, but also between ATKA07 and ATKA11, and between ATKA16 and ATKA21. The sea-ice thicknesses and snow depths recorded by independent manual drillings on the same day are in very good agreement with the EM results in each case (which was expected if a good calibration had been achieved). In general, total thickness continues to grow slowly until December, but first signs of melting can be observed in late December. Especially around ATKA16, small areas of stronger melting start to appear. The melting becomes even more obvious in January, where an overall

thinning of the entire fast ice plus snow can be observed. From the snow measurements (Table 4), which reveal a near constant snow depth until January, it can be inferred that the melting mainly occurred from the bottom. This statement is only true if there wasn't any new snow, which is confirmed by the data from the snow pinger of the AWS(Figure 20). This observation will be investigated in more detail in the future.

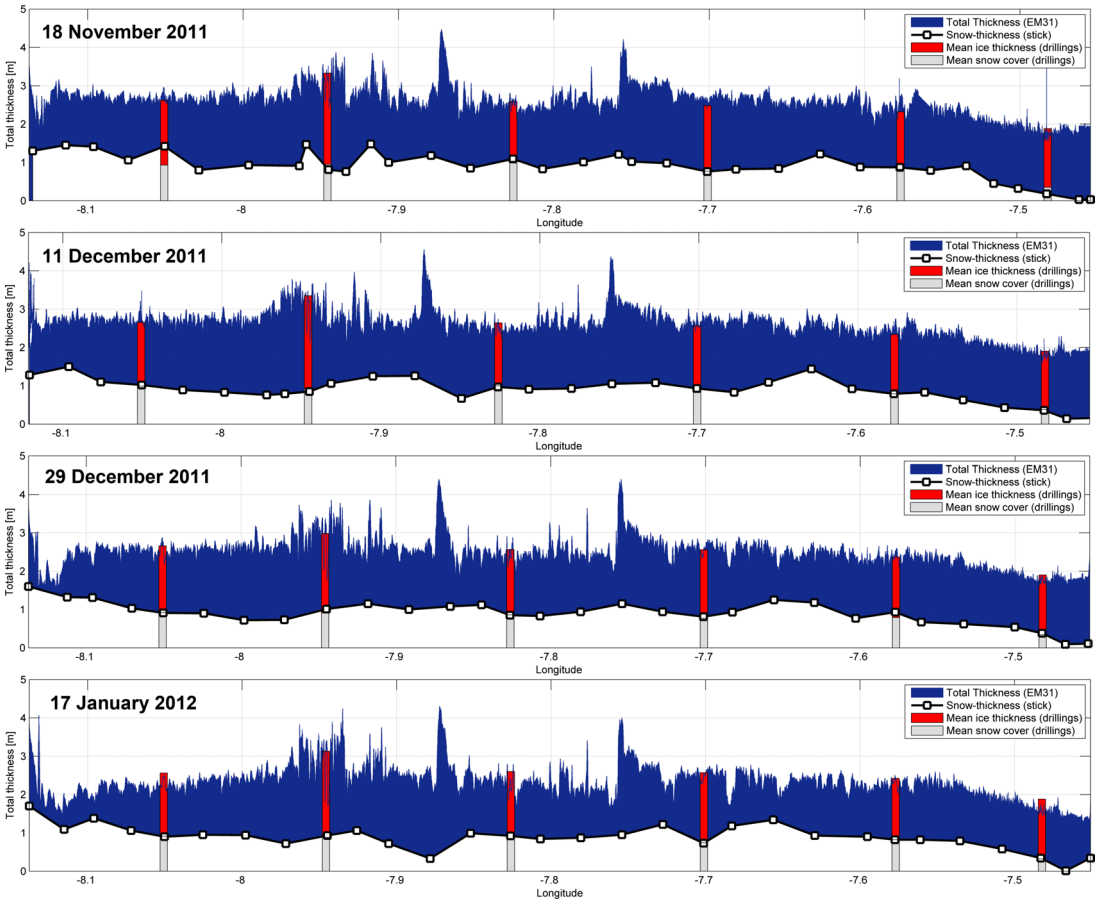

Figure 10: EM31 profiles; Total thickness by EM31 (blue area), snow depth by ruler stick (white area), manual thickness drillings (red bar) and snow depths during drillings (gray bar).

The 114 km thickness data gathered on 29 November 2011 reveal that the total thickness is generally lower by over one quarter in the eastern part. The very thin sea ice measured in the Northeast is suspected to be a result of the vertical coplanar mode mode in which the EM31 was operated, which is not suitable for thicknesses below 1 m. That data is not to be trusted at this point. We plan to operate the EM31 in horizontal coplanar mode to avoid this problem in the future.

But the main advantages of automatic thickness determination with high spatial and temporal resolution (but lower accuracy) by means of EM31 is the possibility to derive a frequency distribution of fast-ice thicknesses as given in Figure 12) for 29 November 2011. This statistical approach yields modes of main thicknesses, two of which can be

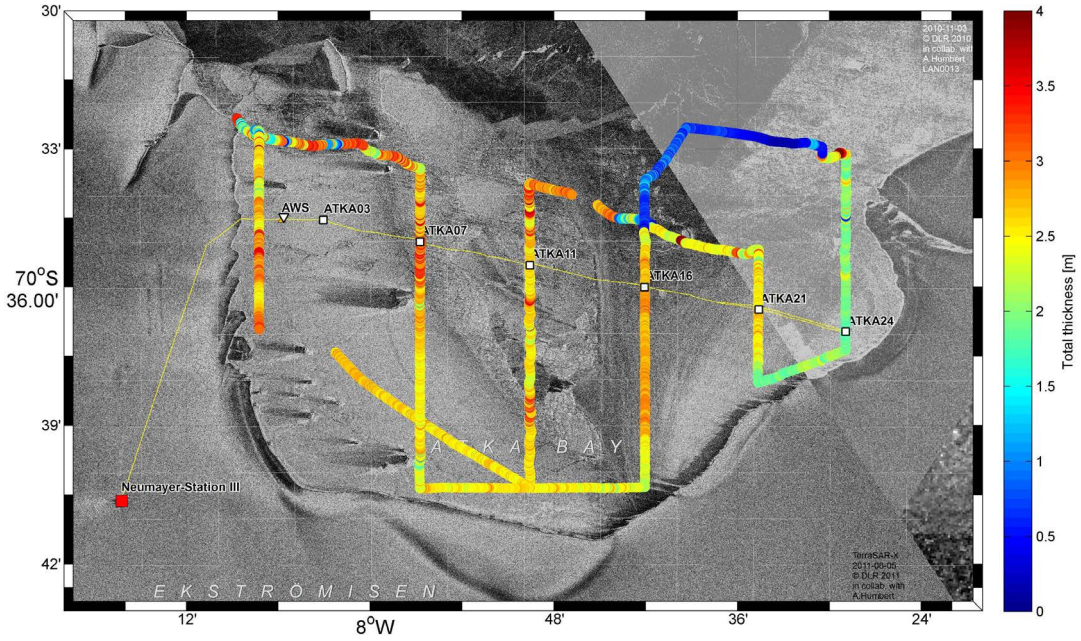

Figure 11: EM31 grid on 29 November 2011

Table 4: Snow depths during EM31 transects. N = number of measurements, z_s = snow depth.

	18.11.2011	29.11.2011	11.12.2011	29.12.2011	17.01.2012
Number	34	65	38	30	30
z_s min [m]	0,03	0,02	0,1	0,09	0,01
z_s max [m]	1,48	1,9	1,52	1,6	1,7
z_s mean [m]	0,91	0,7	0,88	0,9	0,88
z_s std [m]	0,38	0,4	0,37	0,33	0,34

identified from Figure 12a) to be between 0.7 and 0.9 m, as well as at around 2.5 m. The data below 1 m, as stated above, is not trusted at this point. The main modes of manually measured snow depths were around 0.1 m (0.3 m) and 0.9 m, and the probability to find a snow depth over 1 m was below 20 %.

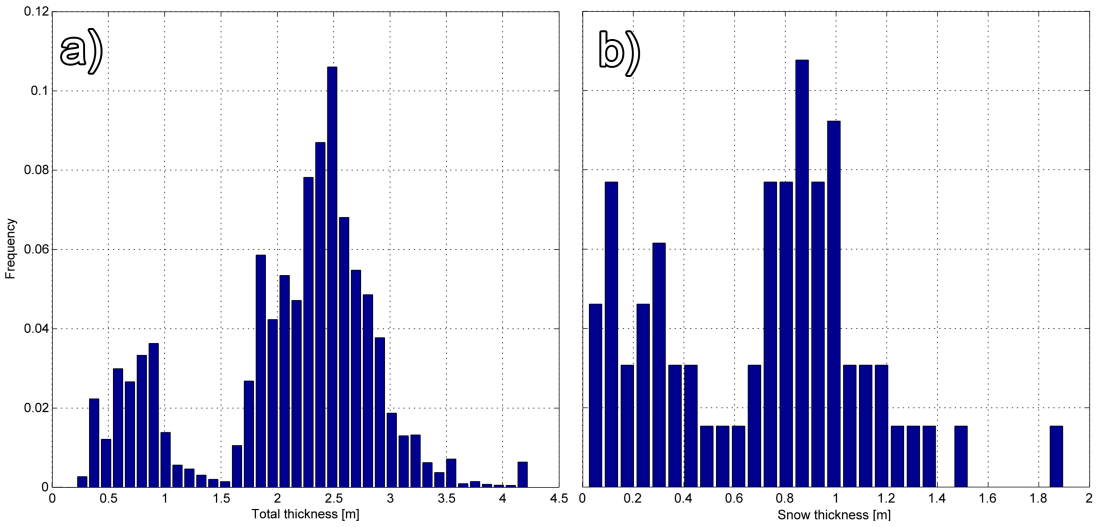

Figure 12: Frequency distribution a) of total thickness; b) snow depths on 29 November

2.3. Snow Density

On 19 August 2011, snow density was measured once at each of the six stations. Snow samples were taken from the snow/sea-ice interface with a cylinder of a fixed volume (451 ml, Figure 13). The weight of the sample minus cylinder was documented and the density was calculated by

$$\rho = \frac{m}{V} \; [\frac{g}{cm^3}]. \tag{3}$$

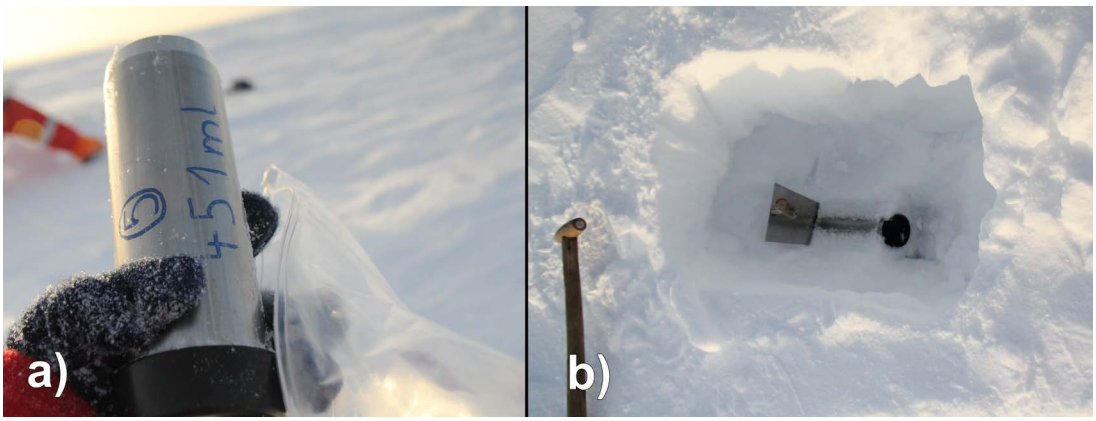

Figure 13: Snow density measurements at sea-ice/snow interface.

Observations

The results of the snow density measurements are shown in Table 5. The highest snow density of 450.1 kg/m^3 was found at ATKA03, where snow depth was generally among the largest during the season. Low densities of around 350 kg/m^3 were measured in the eastern part, where snow depth was constantly among the lowest measured.

Table 5: Results of snow density measurements on 19 August 2011.

Station	Mean snow thickness [m]	Weight [g]	Density [kg/m^3]
ATKA03	0.55	203	450.1
ATKA07	0.32	165,3	366.5
ATKA11	0.50	182,3	404.2
ATKA16	0.46	150,4	333.5
ATKA21	0.42	162,8	361.0
ATKA24	0.32	164,45	364.6

2.4. Automatic Weather Station

On 6 July 2011, an Automatic Weather Station (AWS) was deployed at 70° 34.505' S 8° 05.753' W, 1.6 km from the ice shelf edge (Figure 2). The AWS was configured to measure temperature (2 m), relative humidity, barometric pressure, wind velocity, wind speed as well as downward and upward radiation and snow depth in 1-minute intervals (Figure 14, Table 6).

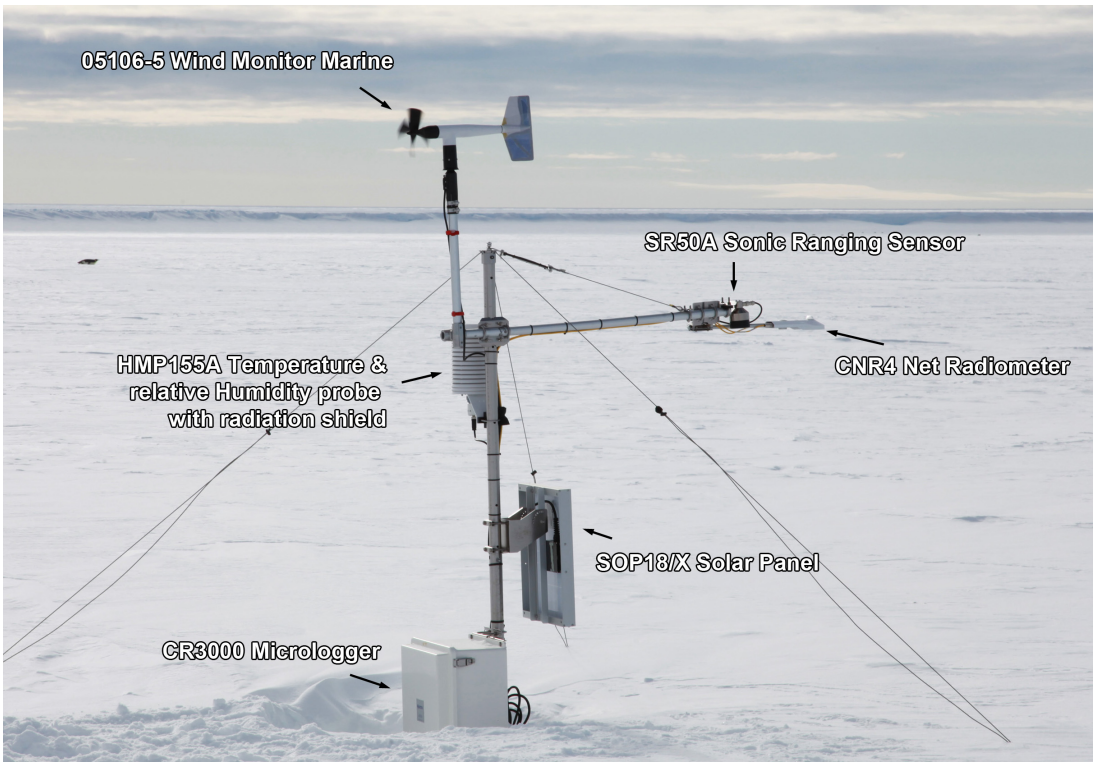

Figure 14: Sensor configuration of Automatic Weather Station

Table 6: Sensors of AWS and measured parameters

Sensor		Measured Parameter
HMP155A	Humicap	temperature, relative humidity
61302V-5A	Barometric pressure sensor	air pressure
05106-5	Wind monitor marine	wind direction, wind speed
CNR4	Net radiometer	bulk long- and short-wavelength radiation
SR50A	Sonic ranging sensor	snow depth

During deployment, the cover of the Humicap sensor broke, leading to data loss of temperature and humidity. It was replaced on 15 July.

Due to a power failure, data is missing between 11 July and 15 July as well as between 26 July and 10 August. Between 10 August and 29 December, the solar panels ensured

a continuous operation. The data was stored on a compact flash card, which was exchanged each time the manual drillings took place.

On 29 December, the AWS was recovered and transported back to Neumayer.

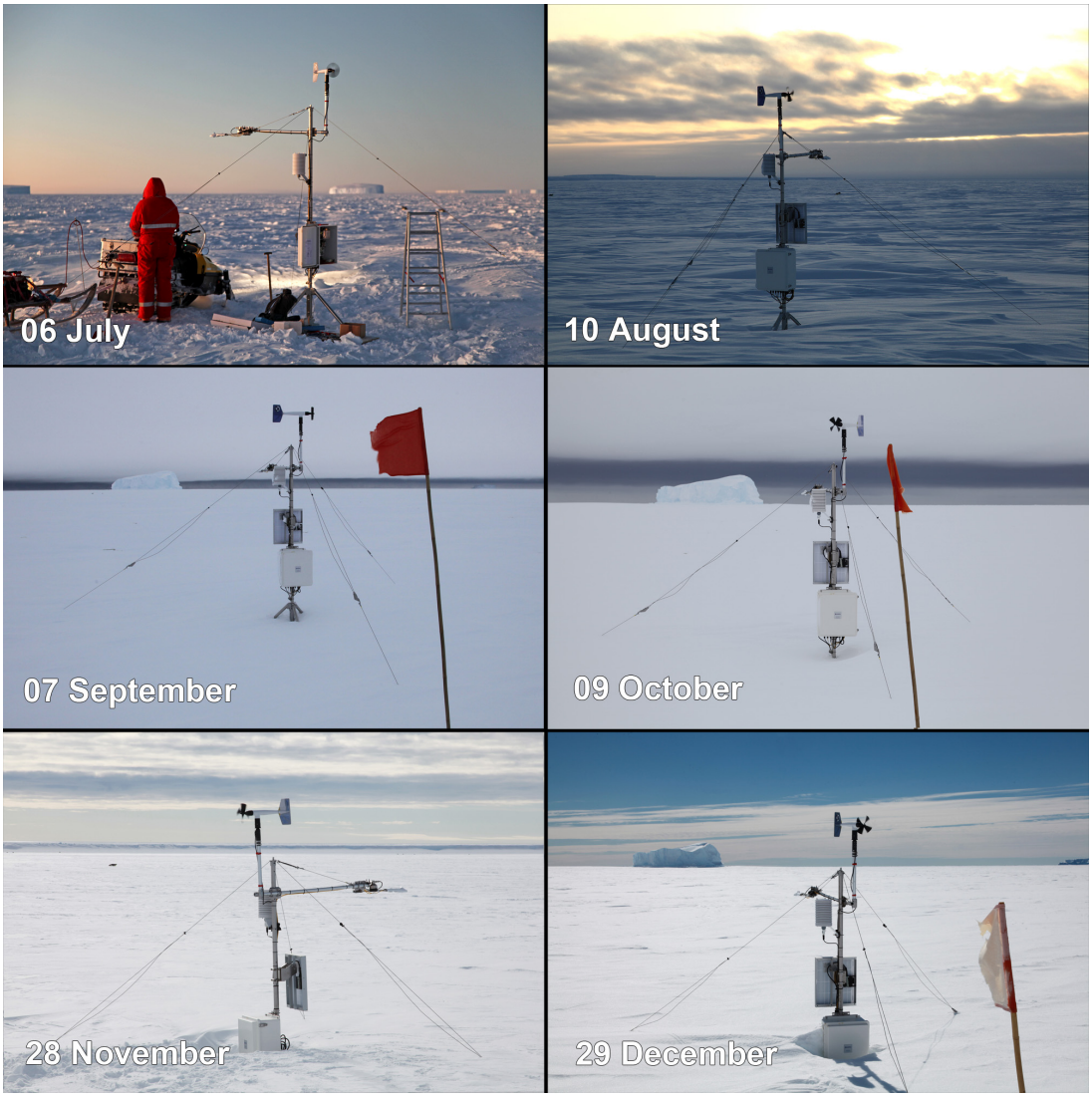

Figure 15: Automatic Weather Station during 2011

Observations

The results of temperature, barometric pressure and relative humidity measurements are shown in Figure 16.

The temperature minimum of -42.23 °C occurred on 21 September, the maximum of 4.77 °C on 18 December. The mean temperature between 10 August and 29 December was -16.54 °C. Atmospheric pressure was highest on 21 July with 1014.5 mbar, and lowest on 09 December with 953.5 mbar. Relative humidity was highly variable and ranged from 44.8 % on 06 November to 97.6 % on 18 December. Humidity may be

strongly influenced by dry katabatic winds and moist oceanic air masses.

Figure 16: Atmospheric conditions at AWS site (Figure 2), measured by Automatic Weather Station in 2011 (gray line) and daily running mean (black line). a) 2m air temperature; b) air pressure; c) relative humidity.

The results of wind direction and wind speed measurements are shown in Figure 17. The wind showed two preferred directions, about 90 ° (easterly winds) and about 250 ° (southwesterly winds). The wind speed was highly variable, but the winds from the East were strongest. The maximum of 29 m/s was measured on 01 November, the mean wind speed was 7.33 m/s.

Results of incoming and outgoing short- and long-wavelength radiation measured by the CNR4 net radiometer are shown in Figure 18.

Daily running mean of upward long-wavelength radiation stays above downward radiation during the entire season. Daily running mean of downward and upward short-wavelength radiation stay close together, which is reflected in high surface albedo values shown in Figure 19. Short term changes in net radiation generally follow the amount of short-wavelength radiation, which is significantly higher than long-wavelength radiation (notice the different scales). This sensor is suspected to be heavily influenced by hoarfrost, so care should be taken in interpreting the results. A future comparison with the BSRN station run at Neumayer III will reveal potential weaknesses of this radiation measurements.

Figure 19 shows the daily mean of albedo, calculated from measured up- and downward short-wavelength radiation. Values below 20 W/m^2 for upward short-wavelength radiation were considered too low and were not included. Between August and October, daily mean albedo varies between 0.54 and 0.98. Between October and January,

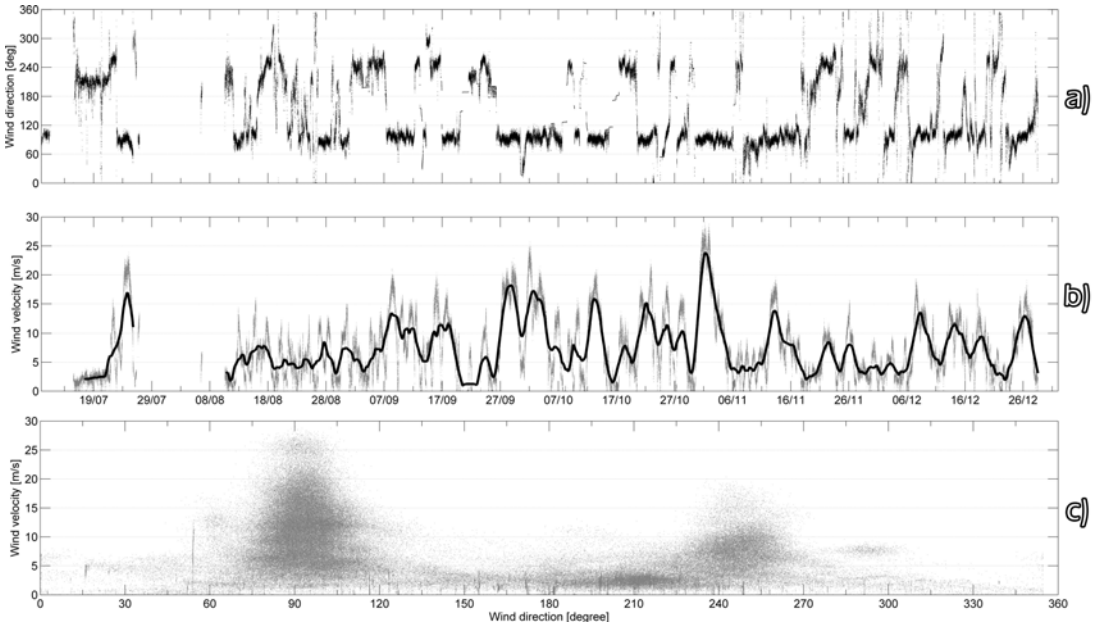

Figure 17: Wind conditions at AWS site (Figure 2), measured by Automatic Weather Station in 2011 (gray line) and daily running mean (black line). a) wind direction (North corresponds to 0°); b) wind velocity ; c) wind speed vs direction.

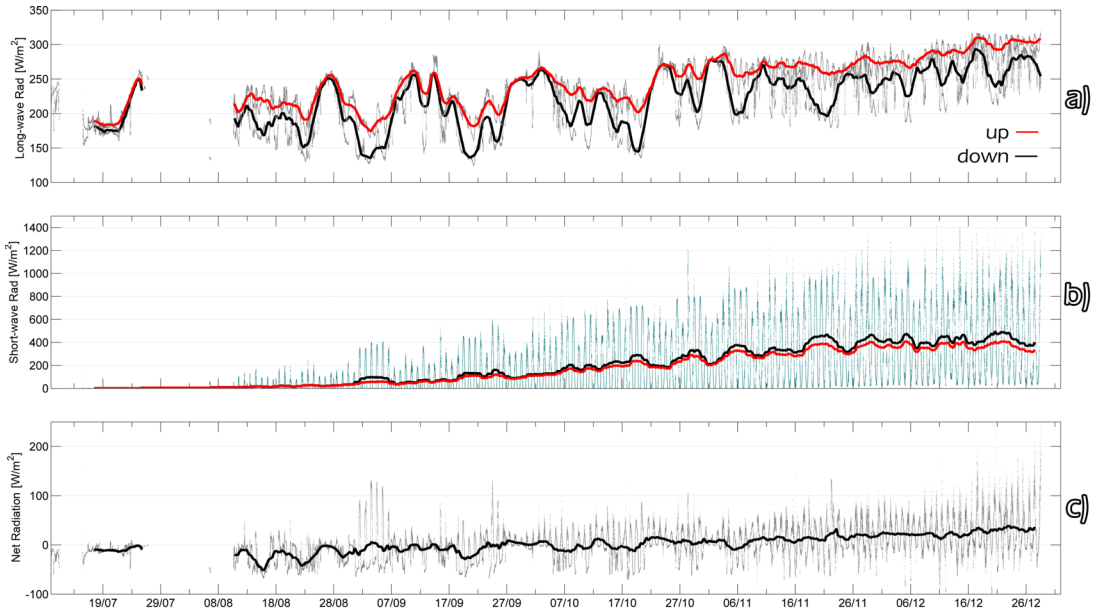

Figure 18: Solar radiation at AWS site (Figure 2), measured by Automatic Weather Station in 2011 (gray line). a) long-wavelength radiation: daily running mean of up- (red line) and downward (black line) long-wavelength radiation; b) short-wavelength radiation: daily running mean of up- (red line) and downward (black line) short-wavelength radiation; c) calculated net radiation (gray) and daily running mean (black line).

the variation becomes less, and the minimum value does not fall below 0.78.

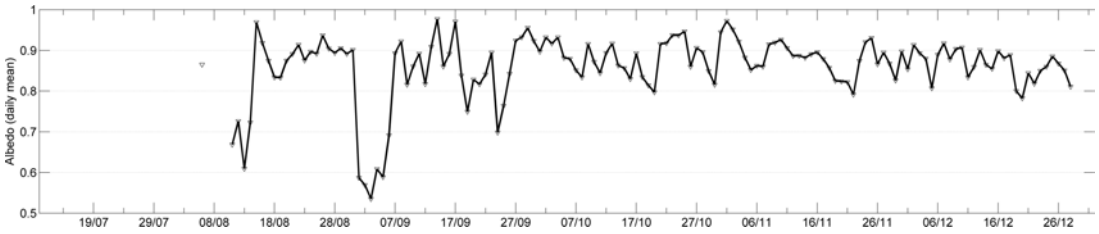

Figure 19: Daily mean of albedo

The temperature-corrected snow depth measured by the ultrasonic snow pinger was smoothed to remove spikes in the data. The resulting time series is presented in Figure 20. Initial snow depth at the time of AWS deployment was about 20 cm. Snow depth increased to about 70cm until the beginning of August, where it stayed constant for 2 month. This result is not reflected in the manual measurements, where snow depth increased at all stations during that time span. In addition, no signs of compaction are visible, which were expected to result in a slight decline of snow depth. Because of this, the data between August and October is not trusted. Between November and January on the other hand, no new snow is deposited at the AWS site, but snow compaction leads to the expected decline in snow depth. At the beginning and at the end of October, snow accumulates during two distinct precipitation events. In the beginning of November, snow depth rises above 2.5 m, which is an unusually high amount not reflected in the manual measurements. This is probably caused by persisting snow storms, driven by easterly winds with speed up to 30 m/s. These result in heavy redistribution of snow and a reflection of the ultrasonic signal at the suspended snow flakes over a long time span. This phenomenon is probably also the cause for spikes in the data, which were removed during data processing and are not shown here.

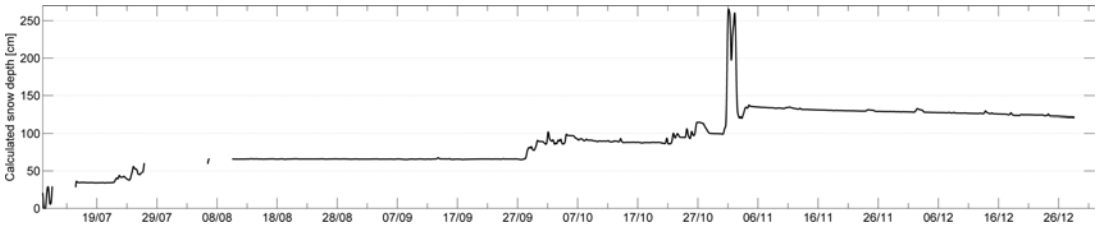

Figure 20: Temperature corrected snow depth at AWS site, measured by ultrasonic snow pinger.

2.5. Thermistor Chain

On 10 August 2011, a thermistor chain Ice Mass-balance Buoy (IMB) designed by the Scottish Association for Marine Science (SAMS) was deployed at the AWS site to measure sea-ice thickness and snow depth in high resolution. and to derive the heat flux through sea ice and snow (Figure 21).

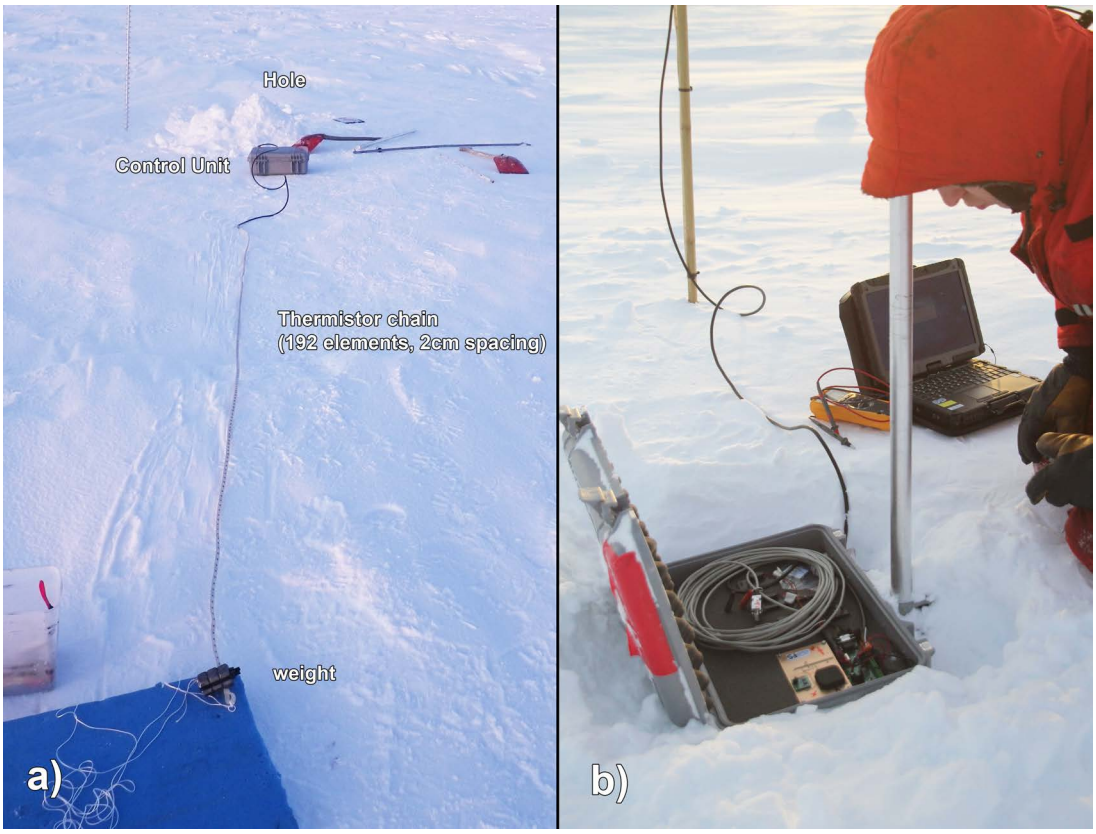

Figure 21: Deployment of SAMS IMB a) the 4 m long chain prior to deployment; b) the control unit is checked for operation.

The device comprised a surface control unit, to which a 3.84 m-long chain of thermistor elements was attached. The 192 thermistors (Maxim DS28EA00 thermometer chips each with a 1 k heater resistor) were spaced at an interval of 2 cm. The chain was lowered through a 5-cm-diameter borehole and frozen into the sea ice such that air, snow, sea ice and water temperatures could be monitored. This device was also able to operate in an "active mode", where the thermistor elements are heated and the temperature rise characteristic is used to determine the type of medium in which each sensor resides. Each chain sensor is controlled by a logging controller and results are reported back regularly using Iridium satellites (SBD mode). The devices are remotely configurable using the same link (Jackson, 2010).

We used a deployment strategy where snow cover is left as undisturbed as possible (Figure 22). At the time of deployment, sea-ice thickness was 1.15 m, snow depth was

0.71 m and freeboard was -8cm. Thermistor numbers at the interfaces are given in Table 7).

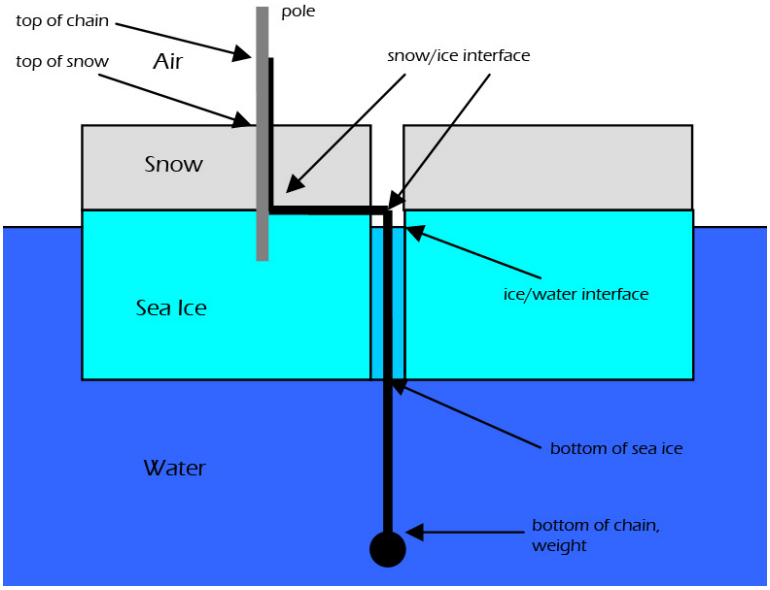

Figure 22: Deployment scheme of SAMS IMB (image after SAMS)

Table 7: IMB sensor numbers at interfaces

Interface	Thermistor number
Top of chain	0
Air/snow	39
Snow/sea ice	74-100
Sea ice/water	158
Bottom of string	192

The temperature and heating data were recovered regularly by reading the integrated compact flash card. Because of an instrument malfunction possibly caused by a damage on the mainboard, data is only available between August 10th and September 15th (with a data gap from 5th to 8th of September), and between November 18th to 28th. Due to the same malfunction, it was not possible to set the measurements at constant intervals. In the end, approximately every 1.5 hours one temperature profile and four heating profiles were recorded. We recovered the instrument on December 29th 2011.

Observations

Figures 23 and 24 show the results of the collected temperature data, but heating data is not shown here. The interfaces of Table 7 can be recognized in Figure 23, and are included as black lines in Figure 24 for clarification. The thermistors at the snow/sea-ice interface sometimes show a temperature difference of several degrees during a single

measurement, which was not expected and remains unclear at this point. Apart from that, the data is consistent with heat conduction models in snow and sea-ice. Between August and November, snow depth has increased by more than 60 cm, which is consistent with the manually measured snow depth. Sea-ice has grown over 60cm, with the sea-ice/water interface nearly reaching the end of the chain.

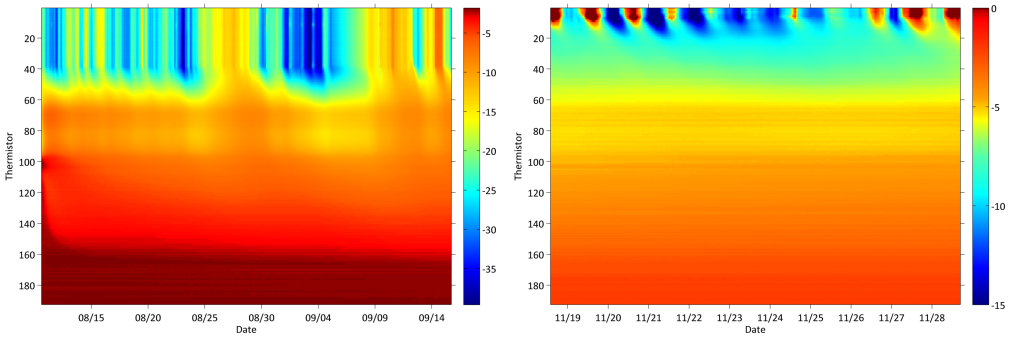

(a) August/September **(b)** November

Figure 23: Temperatures of air, snow, sea ice and water measured by thermistor chain in 2011. Note the different color scales.

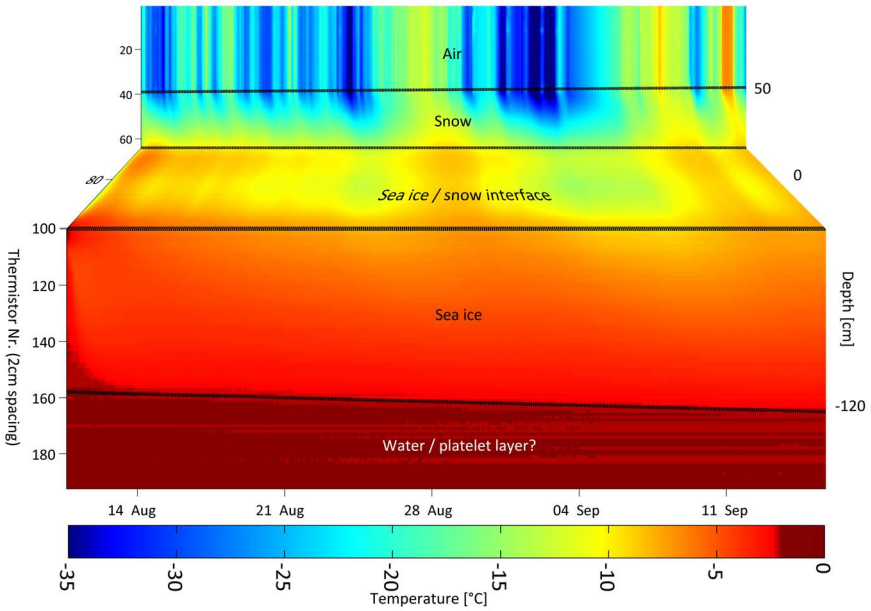

Figure 24: 3-dimensional plot of air, snow, sea ice and water temperatures measured by thermistor chain in August/September. The black lines represent the important interfaces.

2.6. Sea-Ice Cores

Sea-ice cores were retrieved with a Kovacs Mark II coring system (9 cm diameter) from six stations on 29 December 2011 (Figure 25). We recorded a temperature profile of each core with a 10 cm spacing (Figure 26), and stored them in a freezer room at -20°C. Another set of cores were obtained on 17 January 2012, where temperature profiles of each core were taken as well. The transport to Cape Town was scheduled for February 2012, but heavy sea-ice conditions prevented the South African freighter Agulhas to reach the ice shelf edge. As a consequence, the sea-ice cores remain at Neumayer III and are expected to arrive in Bremerhaven in early 2013.

Figure 25: Retrieval of a sea-ice core with a Kovacs Mark II coring system

Figure 26: Measuring the temperature of a sea-ice core

Observations

The temperature profiles of the sea-ice cores retrieved on 29 December 2011 and 17 January 2012 are presented in Figure 27.

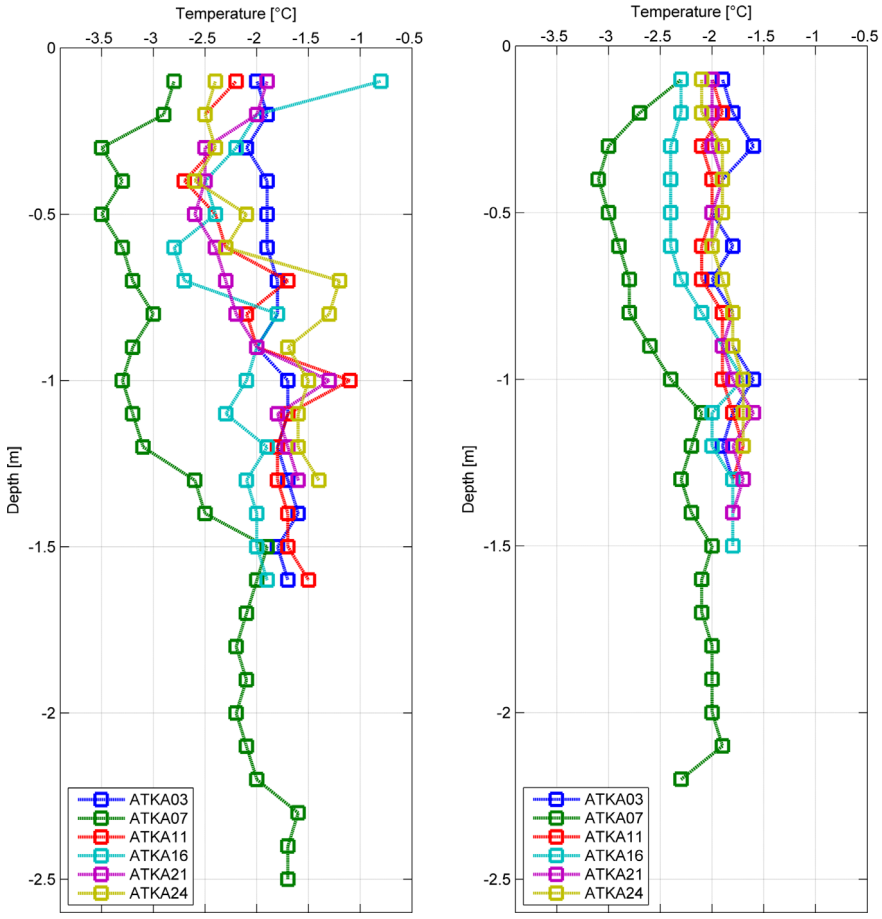

(a) 29 December 2011 **(b)** 17 January 2012

Figure 27: Temperatures measured on sea-ice cores

Once arrived in Bremerhaven, the sea-ice cores will be analyzed with regard to crystal structure and c-axis orientation.

III

Summary

A summary of all data gathered during 2011 is provided in Figure 28 and Table 8.

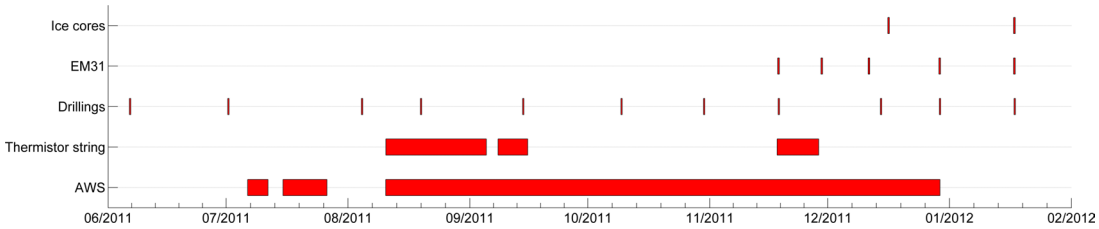

Figure 28: Data gathered on Atka Bay landfast sea ice during our AFIN measurements in 2011.

Table 8: Overview of regular observations. Z_{ice}: sea-ice thickness, Z_{snow}: snow depth, FB: freeboard, T_{ice}: sea-ice temperature, T_{snow}: snow temperature, T_{air}: surface air temperature, P_{air}: air pressure.

Activity	**Parameter**	**Observation frequency**
Thickness transect	Z_{ice}, Z_{snow}, FB	2-4 weeks
EM31 transect	Z_{total}, Z_{snow},	2-4 weeks
Weather station	T_{air}, P_{air}, wind velocity, direction, relative humidity, incoming and outgoing solar irradiance, Z_{snow}	1 min
Mass-balance station	Z_{ice}, Z_{snow}, T_{ice}, T_{snow}, T_{air}	hours
Structural ice cores	Ice structure, T_{ice}, vertical salinity profile	years

Data of manual drillings are deposited at http://doi.pangaea.de/10.1594/PANGAEA.783911, but are password protected at the moment. We are currently working on the upload of other data from this campaign into PANGAEA. Please contact the author for access.

IV
Reference List

Heil, P., Gerland, S. and Granskog, M. A. (2011). An Antarctic monitoring initiative for fast ice and comparison with the Arctic, *The Cryosphere Discussions* **5**(5): 2437–2463.
URL: *http://www.the-cryosphere-discuss.net/5/2437/2011/* (Cited on page 6.)

Hendricks, S. (2009). *Sea-ice thickness with Geonics EM31. Guidelines for Field Experiments and Data Processing.* (Cited on pages 13 and 14.)

Hoppmann, M., Nicolaus, M. and Schmithüsen, H. (2011). Summary of AFIN measurements on Atka Bay landfast ice in 2010.
URL: *http://epic.awi.de/24642/* (Cited on page 7.)

Jackson, K. (2010). *SAMS Ice Mass Balance Array Buoys (SIMBA): Design and Deployment Description.* (Cited on page 24.)

V

Acknowledgements

We are most grateful to Fabian Zahnd, Lisa Kattner, Christian Göbel, Markéta Pokorná, Antje Schlömer, Johannes Lohse and the other overwinterers and helpers at Neumayer III in 2011 for gathering all the data presented in this report.

We thank Angelika Humbert (University of Hamburg) and the German Aerospace Center (DLR) for providing high resolution TerraSAR-X satellite images to plan our campaign.

We highly acknowledge Gert König-Langlo, Bernd Loose, Gerhard Dieckmann, Lars Kindermann and other scientists and technicians at AWI for their support and professional advice in every respect.

We thank Holger Schmithüsen for his help with the meteorological data, and the AWI Logistics for providing us with the fantastic infrastructure.

Further acknowledgements go to Keith Jackson for his help with the thermistor chain, and Geonics for their support regarding the EM31.

The project was partly funded through the German Research Council (DFG) in its priority program "Antarctic Research with comparative investigations in Arctic ice areas" (SPP1158, NI 1092/2).